1nvestigation of 1'ossi)1(! Electromagnetic Disturbances Caused by Spacecraft-1'lasma Interactions at 4 R_S

M. OKADA[1], B.T. '.1'S111 UTA NI', B.E. GOLDSTEIN[2]
11. MATSUMOTO[3], A. 1,. BRINCA[4], and 1'. J. KELLOGG[5]
1 National Institute of 1'olar Research, Japan
2 Jet Propulsion 1 aboratory, USA
3 Radio Atmospheric Science Center, Japan
4 Centro de Electrodinamica, Instituto Superior Tecnico, Portugal
5 School of Physics and Astronomy, University of Minnesota, USA

,11111(' 3. 1995

Abstract

The]1'0]]0S('(1 Small Solar 1'1"01)(" mission features a ("10S(" approach to the sun with a perihelion of' 4 R_s. ('arbon molecules emitted from 1 he spacecraft's heat shield w i 11 become ionized by electron impact and photoionization. The newly created ions and electrons may generate electromagnet ic and electrostat ic plasma waves between LF ($10\Omega_c$) and 1'1,1" ($0.2\Omega_{C2+}$) which are possible sources of interference with in-situ plasma measurements. To understand t his possible int erference, we have perform ed computer simulat ions to model the electroma gnetic and electrostatic field disturbances c aused by t II(1 pick-up p rocess of C_2^+ ions and rel at ed electrons as the spacecra ft flies across t he ext ernal solar coronal magnet ic field. In 01'(1(1 to study the wave particle interact ions, which includes inhomogeneities (of the C_2^+ plasma) and kinetic effects, we use the electromagnet ic part icle code called Kyoto University Electromagnetic Particle Code (KEMPO) [*Matsumoto and Omura*, 1984]. We find that t here are no subst antial plasma waves generated by the electron and ion pickup. The ('1(X1] ic field near t he spacecraft is also small. Th us, there should be no interference for Sn all Sol ar Probe. We will also give a first-principles argument why Low Frequency instabilities should not occur.

1 M odd

A full-particle simulation code is used to study inhomogeneities in a solar wind spacecraft interaction. We use 2-dimensional KEMPO code to solve for the electromagnetic and electrostatic fields and for particle trajectories. This code solves the full set of Maxwell's equations for the electric and magnetic fields and the equation of motion for the particles in the system. They are solved self-consistently based on the particle-in-cell 111('1110(1. Since the KEMPO ('()(1(' treats both ('1(, ctrons and ions as charged particles, it allows us to investigate nonlinear phenomena due to their kinetic effects.

$$\frac{\partial E}{\partial t} = \frac{1}{c^2}\nabla \times B + \mu_o J \tag{1}$$

$$\frac{\partial B}{\partial t} = -\nabla \times E \tag{2}$$

$$\nabla \times B = 0 \tag{3}$$

$$\nabla \times E = \epsilon_o \rho \tag{4}$$

$$\frac{dv}{dt} = q(E + v \times B) \tag{5}$$

$$\frac{dr}{dt} = v \tag{6}$$

Maxwell's equations are solved by a leap frog scheme for time advancement and a centered differential scheme is used for spatial differentiation. The equations of motion for particles are solved with a Buneman-Boris method (*Birdsall et al.* [1985]). In our simulation model (see Figure 1). a half open boundary condition is adopted. That is, damping regions are added in both x boundaries and periodic boundary conditions are used in the y direction. The plasma \\'ii"\'(s propagating in the x direction are damped near the edges of the simulation box (see Figure 1) and particles are not traced beyond the $x = 0$, x_{max} boundary. x_{max} represents the size of the system including the damping regions. At the center of the system we put in an internal boundary which ("Ol'l'(,S])01) (1S" 10 the spacecraft. This is indicated by the shaded box of size $2R_o$. In this model all particles impinging upon the spacecraft sill'f;l(e are absorbed. that is, the reflection coefficient of the particles at the spacecraft Sill'lil(.(, is assumed to be 7,(,1'(). The potential of the spacecraft is calculated from the accumulated charge using a capacitance matrix method [*Hockney and Eastwood*, 1988]. The solar wind flows along x axis from left-to right and the solar wind magnetic field has an angle θ relative to the flow direction and lies within the x - y plane. We ('1100S(" the spacecraft as our frame of" reference. The external electric field has an intensity of $v_d \times B_o$. This is ill the z direction, e. g., into the paper. In order 10 simulate an open boundary system, the solar wind particles are injected from both ends (because (If the large thermal velocities, some particles enter the box from the right side), $x = 0$, x_{max} , with a constant ambient flux which is calculated from the thermal velocity and the solar wind velocity v_{sw}.

Table 1 gives the 11)() (1(,1 parameters. We find the electron beta, ion sound Mach number and Alfvén mach number are 0.013, 5.0 and 0.4, respectively. Note that the flow speed is supersonic but not super-Alfvénic. The characteristic frequencies of each species are ('110 S('11 t o maintain realistic ratios relative t o the ('1('('t ron ('j'("lot ron frequency. The drift, ion thermal and ion sound velocities are indicated with a value normalized to the solar wind electron thermal velocity. Solar wind (,I((fl'oils and ions are considered to be isothermal.

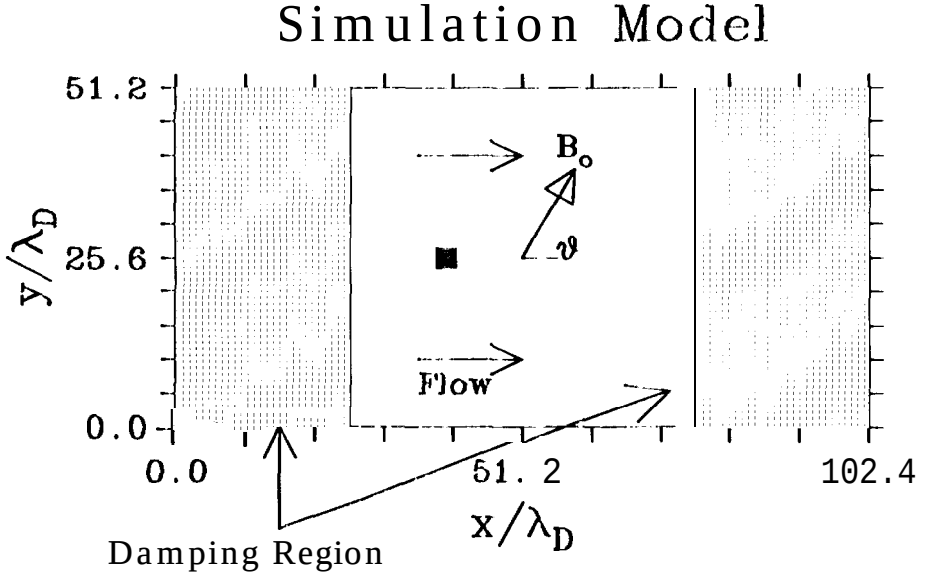

Figure 1: Simulation model

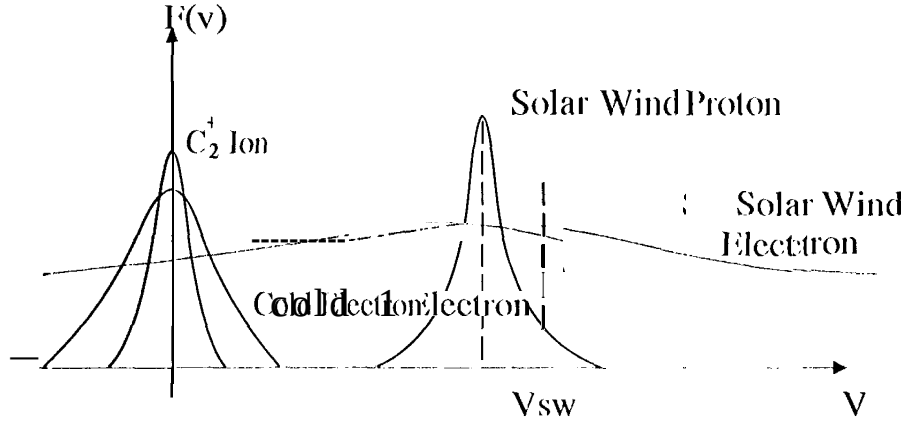

Figure 2: Velocity distribution function used in the computer experiments.

The mass ratios of the electrons, protons and C_2 ions are assumed to be 1:16:100 in our simulation. The mass ratio is necessary for reasons of computational efficiency. The thermal velocity of C_2-origin ions is assumed to be 10 times smaller than that of solar wind electrons. The thermal velocity of C_2 ions is very small, and therefore the ions can be assumed to be a cold beam in the solar wind. Figure 2 shows the velocity distribution function used in the computer simulations.

2 Results

We perform 4 computer simulation runs with different values of the angle of the external magnetic field relative to the solar wind flow direction and C_2 densities. Parameters for each simulation run are listed in Table 2. We first perform a 30° simulation without C_2 particles (θ = 30°) to identify what kind of

waves are generated due to the spacecraft-solar wind interaction without pickup ions present. We do this for baseline information. Next we put the C_2 pickup plasma into the system and compare the difference between two cases at four different θ values (θ = 0°, 30°, 60° and 90°). The larmor radius is 200 λ_D, larger than the simulation box, 51.2 λ_D.

The 4 Figures (Figures 4, 5, 6 and 7) illustrate the densities when C_2 ions are present. Figure 4 is the case where the external magnetic field has an angle of 0° relative to the solar wind flow direction. The density profiles of the solar wind electrons (a), protons (b), C_2-origin electrons (c) and C_2^+ ions (d) are shown, respectively. A solar wind ion wake is formed behind the spacecraft (see panel (b)). This is primarily caused by the C_2 ion density enhancement near the spacecraft (shown in panel (d)), displacing solar wind protons. There is a C_2 ion density buildup in the vicinity of the spacecraft (panel (d)). The largest densities are on the upstream side of the spacecraft. While the newly created C_2^+ ions are removed slowly from the vicinity of the spacecraft, the C_2-origin electrons are carried away very fast by interacting with the solar wind electrons.

There is also a small region of downstream C_2^+ density enhancement just behind the spacecraft. The cause of this enhancement is a charge separation in the wake region of the spacecraft. The C_2^+ ions are trapped by the potential well caused by this charge separation of the solar wind protons and electrons.

As the angle of the magnetic field relative to the spacecraft velocity increases (Figures 5 to 7) more C_2 electrons are carried away from the spacecraft. The C_2 ions again build up on the upstream side of the spacecraft. For the θ = 30° case, the absolute densities are almost the same as the θ = 0° case, but the C_2^+ ion density structure is now much broader in angle. Note the $\boldsymbol{E} \times \boldsymbol{B}$ flow direction is from the upper left to lower right and therefore the asymmetry in the C_2^+ ions in the y direction. There is again a high-density, narrow downstream enhancement region. There is a charge separation electric field caused by electron mobility along $\boldsymbol{B}$ near the edges of the wake.

Figure 7 represents the solar wind and C_2 plasma density with the same format as the previous figure but for θ = 90°. Because of the orthogonal field orientation, the C_2^+ density enhancement in the upstream region is now symmetric about the y direction. There is also now a lack of an enhancement in the downstream region.

Figure 3 depicts the potential structure around the spacecraft with a bird's eye view for the θ = 90° case. A potential hill due to charge separation exists behind the spacecraft. The potential of the spacecraft itself is not affected much by spacecraft charging effects. The potential of the spacecraft is almost -2.6×10^{-2} of the electron thermal energy ($\kappa_B T_e$). The corresponding electric field at the spacecrecraft surface over the Debye length is $\sim 5.2 \times 10^{-2}$ V m^{-1}, 2 orders of magnitude lower than the $v_d \times B_o$ electric field. To understand this potential, we have run the simulation without carbon ions present. This potential is caused by the C_2^+ ions in the vicinity of the spacecraft. The maximum of this potential kept low due to the presence of background thermal electrons. The maximum of this potential is $\sim -2.6 \times 10^{-2} \kappa_B T_e \sim 5.0eV$. The drift energy of the solar wind proton is $\sim 00eV$. Thus, this should not lead to any interference with solar wind plasma detection.

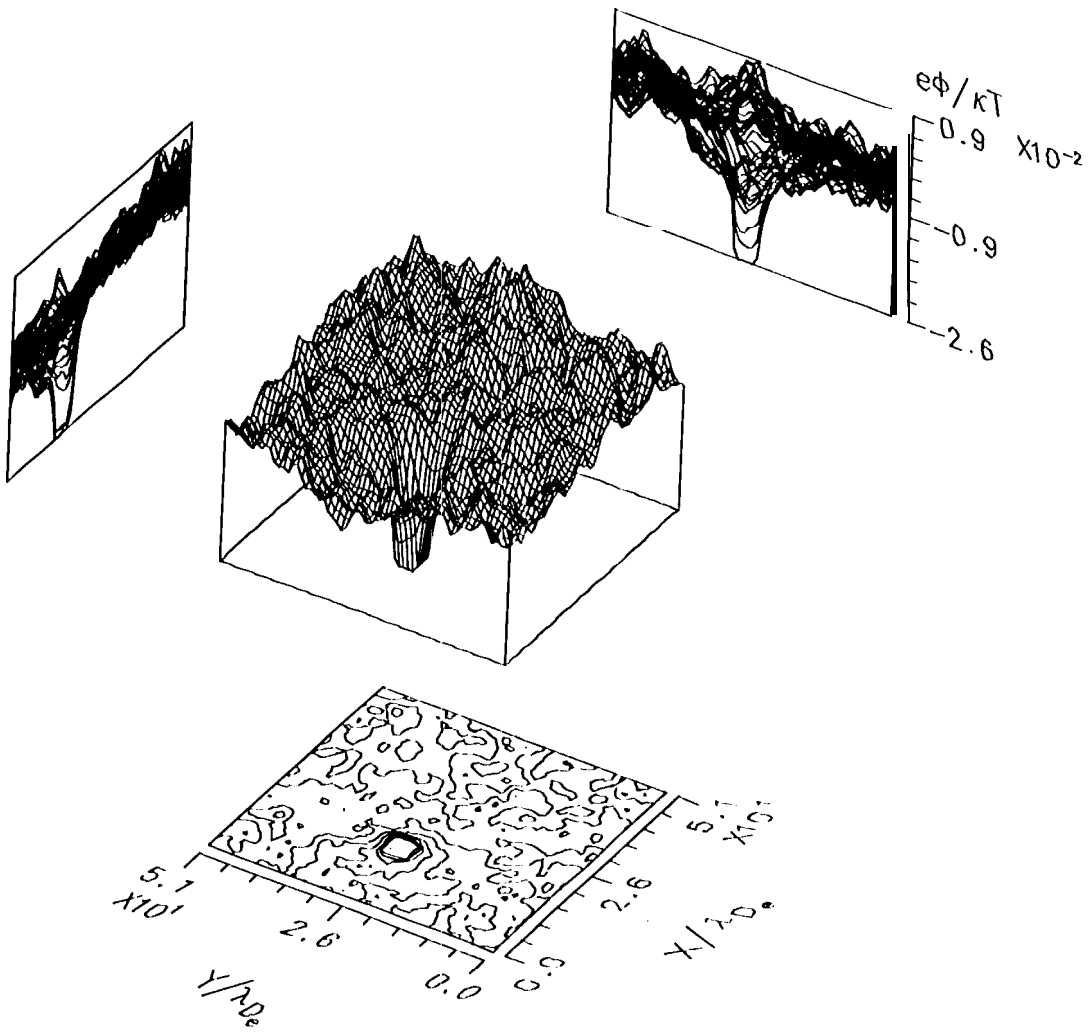

Figure 3: Potential structute around the spacecraft

3 Summary

We have performed 4 computer simulations, one without C_2 ions and others with C_2 ions and $\theta = 0°, 30°$ and $90°$.

There is an upstream C_2^+ density feature for all cases of θ. The density enhancement has a magnitude of $\sim 4n_o$. This density enhancement is caused by the charge separation of C_2^+ ions and electrons. This spatial structure is commonly seen for all cases of θ. The shape of this density feature is depend on θ. This is due to the $\boldsymbol{v}_{sc} \times \boldsymbol{B}$ drift of the ions, where $\boldsymbol{v}_{sc}$ is the spacecraft velocity. There is negligiblie potential near the spacecraft on the solar side. There is a measureable spacecraft potential but quite small $\sim 5.2 \times 10^{-2}$ V m^{-1}. We also compared the peak energy of the potential structure with the drift energy of the solar wind protons. We confirmed that the solar wind flow is not affected by this potential.

We also checked the wave intensity in the vicinity of the spacecraft. We could not find any change in the frequency spectrum due to the C_2^+ plasma

References

[1] Al'pert, Y. L., Space plasma, Cambridge Univ. Press, 990

[2] Birdsall, C. K. and A. B. Langdon, Plasma physics via computer simulation, *MacGraw-Hill*, 1985

[3] Brinca, A. L. and B. T. Tsurutani, Influence of multiple ion species on low-frequency electromagnetic wave instabilities, *J. Geophys. Res.*, **94**, 13565, 1989.

[4] Goldstein, B. E., W. C. Feldman, H. B. Garrett, Katz, L. Linson, K W. Ogilvie, F. L. Scarf and E. C. Whipple, Spacecraft mass loss and electric potential requirements for the starprobe mission, J PL 715-100, 980

[5] Hockney, W., J. W. Eastwood, Computer simulation using particles, *Adam Hilger, Bristol and Philadelphia*, 1988

[6] Matsumoto, H., K. Inagaki and Y. Omura, Computer simulation of passage of an electron beam through a plasma, *Adv. Space. Res.*, **8**, pp.151-160, 988.

[7] Matsumoto. H. and Y. Omura, Particle simulation of electromagnetic waves and its application to space plasmas, *Computer Simulation of Space Plasmas*, I. Matsumoto and T. Sato, pp.43 02, Terra Scientific Publishing Company, 1984.

[8] Omura, Y., and . Matsumoto, Computer experiments on whistler and plasma wave emission for space lab-2 electron beam", *Geophys. Res. Lett.*, **15**, 319-322. 1988.

[9] Tsurutani, B. T., COMETS: A laboratory for plasma waves and instabilities, *AGU*, Geophysical Monograph 61, 1991

The research described in this publication was carried out by the Jet Propulsion Laboratory, California Institute of Technology, under a contract with the National Aeronautics and Space Administration.

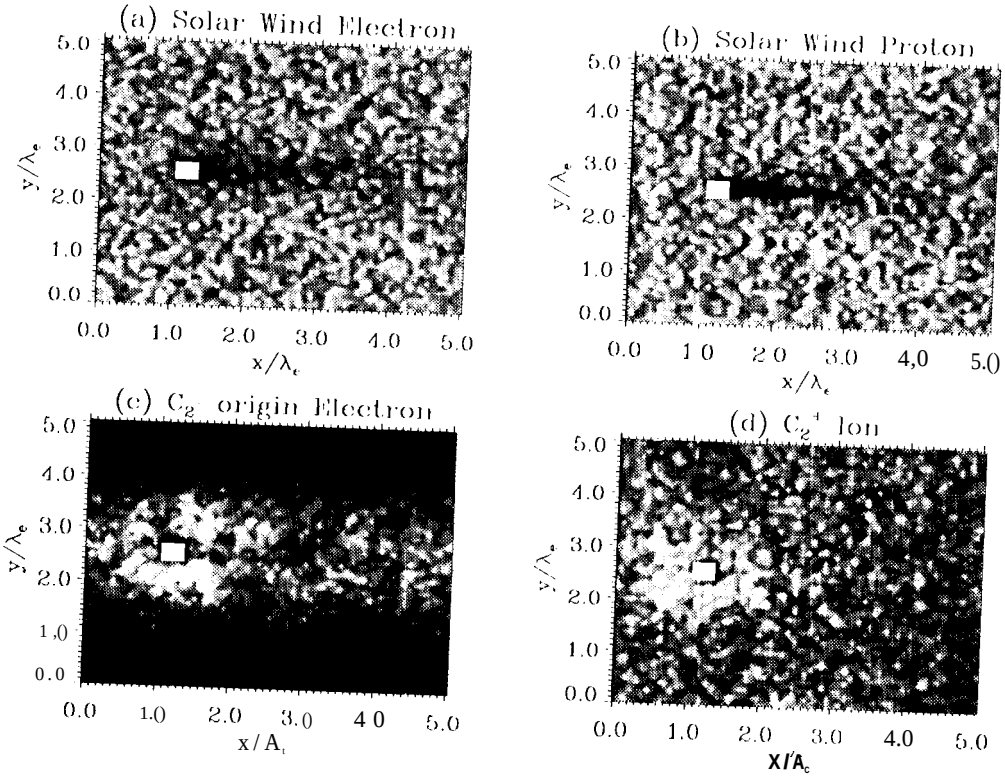

Figure 4: Plasma particle number density contour in the case where $\theta = 0^o$.

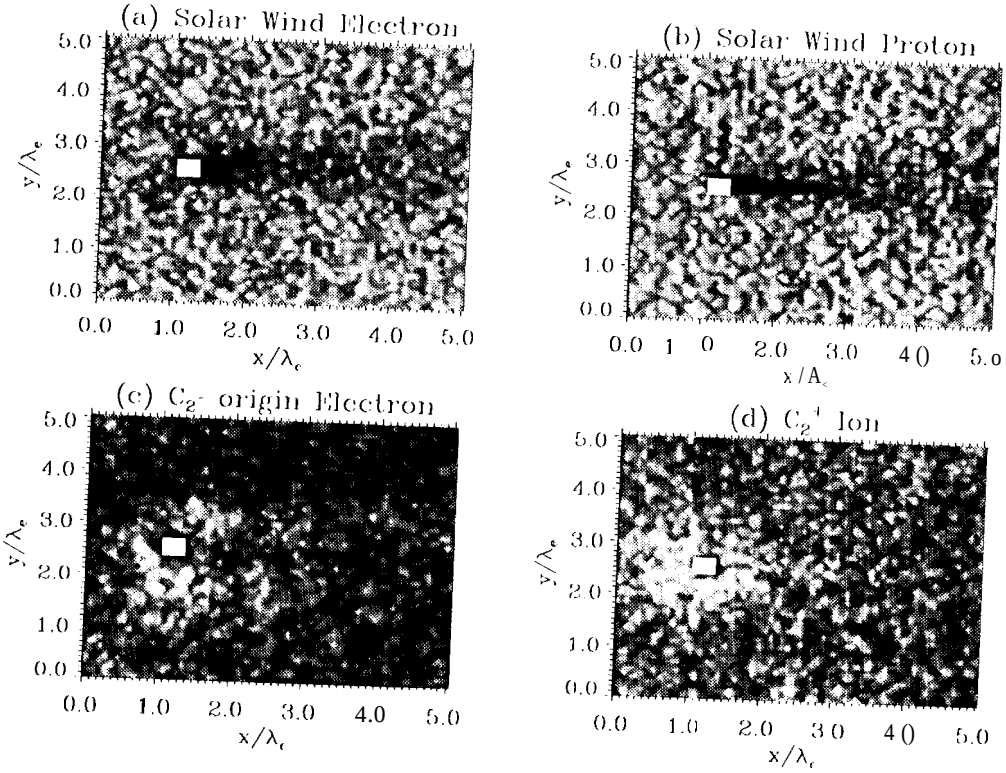

Figure 5: Plasma particle number density contour in the case where $\theta = 30^o$.